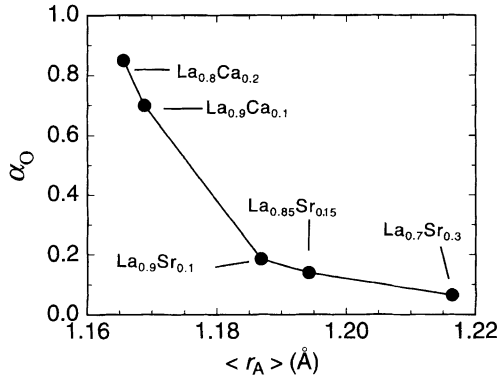

FIG. 3 The dependence of the oxygen isotope exponent α_O on the average ionic radius $\langle r_A \rangle$ at the cation site $La_{1-x}Me_x$. (The results for the Sr-doped compounds are unpublished results of G.M.Z. and D. E. Morris.) The solid line is to guide the eye. The isotope exponent α_O increases rapidly with decreasing $\langle r_A \rangle$.

constants of the two isotope samples[13]. For the present CMR materials, we have used the same oxygen-isotope exchange procedure as for the $La_{2-x}Sr_xCuO_{4+y}$ compound, so we expect that the oxygen contents of the present ^{16}O and ^{18}O samples are the same as well.

We now consider why the oxygen isotope exponents α_O in Ca-doped $La_{1-x}Ca_xMnO_{3+y}$ are much larger than those in Sr-doped $La_{1-x}Sr_xMnO_{3+y}$. This may be due to the difference in the ionic radii of Ca^{2+} and Sr^{2+}. In Fig. 3 we show the dependence of α_O on the average ionic radius $\langle r_A \rangle$ at the cation site $La_{1-x}Me_x$. The ionic radii of $La_{1-x}Me_x$ were calculated from tabulated values (La^{3+}, 1.172 Å; Ca^{2+}, 1.140 Å; Sr^{2+}, 1.320 Å; ref. 14). It is evident that α_O increases rapidly with decreasing $\langle r_A \rangle$. Although α_O may also depend on the Mn^{4+} concentrations, it is clear from Fig. 3 that $\langle r_A \rangle$ has a dominant effect on the value of α_O. A similar correlation between the magnitude of the magnetoresistance and $\langle r_A \rangle$ has recently been reported by Hwang *et al.*[15]; they showed that the magnetoresistance decreases rapidly with increasing $\langle r_A \rangle$. Thus, the oxygen-isotope exponent α_O is correlated with the magnitude of magnetoresistance.

As there is no oxygen-isotope effect on T_c in the ferromagnet $SrRuO_3$ which has a negligible JT effect, the giant isotope effect observed in the Ca-doped ferromagnets is very likely to be related to the strong JT effect in this system. For a compound with a strong JT effect, the electron–phonon interaction is also large, leading to the formation of JT polarons[6]. Taking into account that the binding energy of polarons E_b in the JT compound is equal to the JT stabilization energy E_{JT} (ref. 8), and $T_c \propto W_{eff}$ for $J_H \gg W_{eff}$, equation (1) gives

$$T_c \propto W \exp(-\gamma E_{JT}/\hbar\omega) \quad (2)$$

The total isotope exponent is then given by

$$\alpha = -\mathrm{d}\ln T_c/\mathrm{d}\ln M = 0.5\gamma E_{JT}/\hbar\omega \quad (3)$$

Because γ increases with increasing E_{JT}/W (ref. 7) equation (3) indicates that the isotope exponent increases with increasing E_{JT}, but decreases with increasing W. For the manganites, an increase in $\langle r_A \rangle$ usually enhances the covalency of the Mn–O bonding[16], and hence increases the bare conduction bandwidth W, leading to a decrease of α. This mechanism naturally explains why the oxygen-isotope exponent α_O increases with decreasing $\langle r_A \rangle$, as shown in Fig. 3.

Our results thus strongly suggest that in the CMR manganites there is a substantial JT effect and thus a large electron–phonon interaction which leads to the formation of JT polarons[6]. This is also consistent with a recent theoretical study of the JT lattice coupling effects in the CMR manganites[17]. For the ferromagnet $SrRuO_3$ with a negligible JT effect, the electron–phonon interaction may be very small, so that no polarons are formed. That is why no oxygen isotope effect on the Curie temperature is observed in the ferromagnet $SrRuO_3$. □

Received 8 March; accepted 9 May 1996.

1. Jin, S. *et al. Science* **264,** 413–415 (1994).
2. Jonker, G. H. & Van Santen, J. H. *Physica* **16,** 337–349 (1950).
3. Chahara, K. *et al. Appl. Phys. Lett.* **63,** 1990–1992 (1993). **(see note below)**
4. Jahn, H. A. & Teller, E. *Proc. R. Soc. Lond. A* **161,** 220–235 (1937).
5. Anderson, P. W. & Hasegawa, H. *Phys. Rev.* **100,** 675–681 (1955).
6. Höck, K.-H., Nickisch, H. & Thomas, H. *Helv. phys. Acta* **50,** 237–243 (1983).
7. Alexandrov, A. S. & Mott, N. F. *Int. J. mod. Phys.* B**8,** 2075–2109 (1994).
8. De Jongh, L. J. *Physica* C**152,** 171–216 (1988).
9. Millis, A. J., Littlewood, P. B. & Shraiman, B. I. *Phys. Rev. Lett.* **74,** 5144–5147 (1995).
10. Shikano, M. *et al. Solid St. Commun.* **90,** 115–119 (1994).
11. Zech, D. *et al. Nature* **371,** 681–683 (1994).
12. Schiffer, P. *et al. Phys. Rev. Lett.* **75,** 3336–3339 (1995).
13. Zhao, G. M. *et al. Phys. Rev.* B**52,** 6840–6844 (1995).
14. Shannon, R. D. *Acta crystallogr.* A**32,** 751–767 (1976).
15. Hwang, H. Y. *et al. Phys. Rev. Lett.* **75,** 914–917 (1995).
16. Goodenough, J. B. *Phys. Rev.* **106,** 564–573 (1955).
17. Röder, H., Zhang, J. & Bishop, A. R. *Phys. Rev. Lett.* **76,** 1356–1359 (1996).

ACKNOWLEDGEMENTS. This work was supported by the Swiss National Science Foundation.

Exceptionally high Young's modulus observed for individual carbon nanotubes

M. M. J. Treacy*, T. W. Ebbesen* & J. M. Gibson†

*NEC Research Institute, Inc., 4 Independence Way, Princeton, New Jersey 08540, USA
† University of Illinois, Department of Physics, 1110 West Green Street, Urbana, Illinois 61801, USA

Carbon nanotubes are predicted to have interesting mechanical properties—in particular, high stiffness and axial strength—as a result of their seamless cylindrical graphitic structure[1–5]. Their mechanical properties have so far eluded direct measurement, however, because of the very small dimensions of nanotubes. Here we estimate the Young's modulus of isolated nanotubes by measuring, in the transmission electron microscope, the amplitude of their intrinsic thermal vibrations. We find that carbon nanotubes have exceptionally high Young's moduli, in the terapascal (TPa) range. Their high stiffness, coupled with their low density, implies that nanotubes might be useful as nanoscale fibres in strong, lightweight composite materials.

Large bundles of carbon nanotubes were teased from a core

TABLE 1 Properties of individual nanotubes

Nanotube no.	Length (μm)	Outer diameter (nm)	Inner diameter (nm)	Young's modulus (TPa)
1	1.17	5.6	2.3	1.06
2	3.11	7.3	2.0	0.91
3	5.81	24.8	6.6	0.59
4	2.65	11.9	2.0	1.06
5	1.73	7.0	2.3	2.58
6	1.53	6.6	2.3	3.11
7	2.04	7.0	3.0	1.91
8	1.43	6.6	3.3	4.15
9	0.66	7.0	3.3	0.42
10	1.32	9.9	3.0	0.40
11	5.10	8.4	1.0	3.70

Average value of Young's modulus is 1.8 TPa.

deposit, which had been prepared by the carbon arc method[1,6], and attached to the edge of a hole in 3-mm-diameter nickel rings for transmission electron microscopy (TEM) observations. The tip of the fibrous bundle was gently shredded by pulling with tweezers to produce a brush of roughly horizontal isolated nanotubes, which are effectively clamped at one end. The specimens were examined in a Hitachi H9000NAR TEM at 100 kV, and were supported on a Gatan 652-Ta side-entry heating holder equipped with a thermocouple. A Gatan model 690 slow-scan CCD (charge-coupled device) camera, in conjunction with Digital Micrograph v2.5 software, was used to collect and process image data.

In the TEM at room temperature, it was found to be impossible to focus on the tips of the longest and thinnest nanotubes. The images were significantly blurred at the free ends, but could be brought sharply into focus at the supported ends. Refocusing demonstrated that the tip blurring was not caused by focal gradients due to nanotubes being inclined to the optic axis. Increasing the specimen temperature to 600 K significantly increased the blurring at the tips. This result indicates that these nanotubes are vibrating, and that the vibration is of thermal origin. Figure 1 compares the bright-field images of several micrometre-long nanotubes at 300 and 600 K. Near the supported base they measure ~15 nm across. At the tips, however, image contrast is lower. At 300 K the imaged tip width of one of them is ~30 nm, whereas at 600 K the width is ~40 nm. Decreasing the electron beam current density by a factor of 1,000 does not noticeably affect the motion. Detailed measurements of the vibration amplitude with temperature (Fig. 2) confirm the thermal origin. Occasionally, nanotubes are observed with relatively massive lumps attached near their end (see, for example, the nanotube on the right of each panel in Fig. 1). These weighted nanotubes sway and twitch laterally in a random manner that is suggestive of brownian motion.

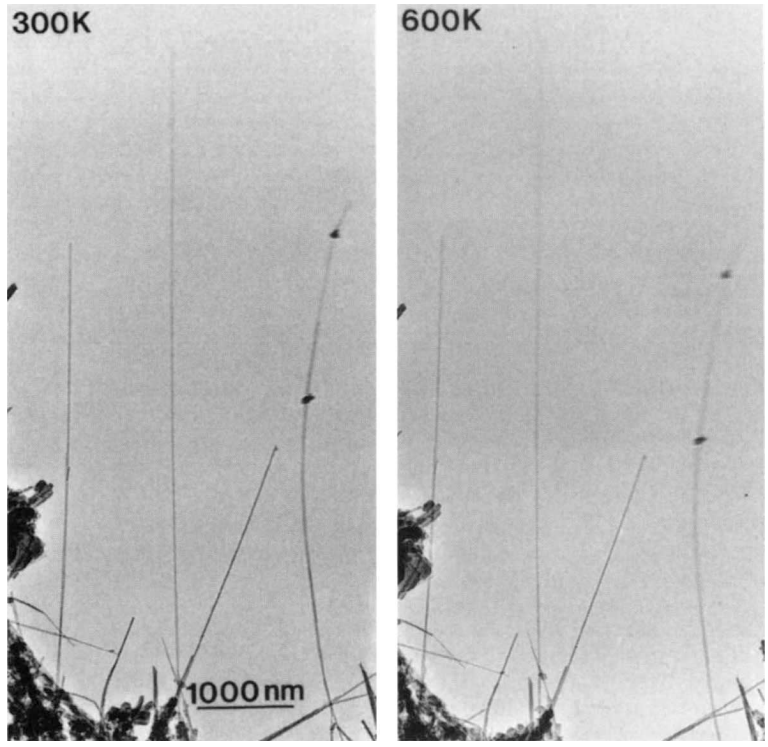

FIG. 1 Bright-field TEM micrographs of free-standing carbon nanotube fibres showing the blurring at the tips due to thermal vibration. Left panel, 300 K; right panel, 600 K.

We assume that a nanotube is equivalent to a clamped homogeneous cylindrical cantilever of length L, with outer and inner radii a and b, respectively. It can be shown that for a given mode, n, the horizontal vibration amplitude at the tip, u_n, is related to the Young's modulus Y and the vibration energy W_n through[7]

$$W_n = \frac{1}{2} c_n u_n^2 \tag{1}$$

where the effective spring constant for the motion of the tip is

$$c_n = \frac{\pi \beta_n^4 Y(a^4 - b^4)}{16L^3} \tag{2}$$

The values of β_n are found from the solutions to the equation $\cos\beta \cosh\beta + 1 = 0$. $\beta_0 \approx 1.8751$ for the fundamental mode, and $\beta_1 \approx 4.6941$, $\beta_2 \approx 7.8548$, $\beta_3 \approx 10.9955$ for the first three overtones. $\beta_n \approx (n + 1/2)\pi$ for larger n. The undamped vibration frequency is[3]

$$\omega_n = 2\pi f_n = \frac{\beta_n^2}{2L^2} \sqrt{\frac{Y(a^2 + b^2)}{\rho}} \tag{3}$$

where ρ is the density of the material in the nanotube wall. For typical nanotubes at room temperature, we expect $\omega_0 \approx 10^7$ Hz, and $kT \gg \hbar\omega_n$ for $n \leqslant 1{,}000$. Consequently, from the law of equipartition, there is an average energy of $kT/2$ per degree of freedom for all of the relevant lateral vibration modes. Because there are both elastic and kinetic energy degrees of freedom for all of the relevant lateral vibration modes. Because there are both elastic and kinetic energy degrees of freedom in a vibrational mode then, on average, $\langle W_n \rangle = kT$ for each vibration mode, with W_n obeying the Boltzmann distribution. It is straightforward to show that each mode of a stochastically-driven oscillator has a gaussian vibration probability profile, with standard deviation given by $\sigma_n = (kT/c_n)^{1/2}$. As the modes are mutually independent, the vibration profile for the combined modes is also a gaussian, with standard deviation given by the

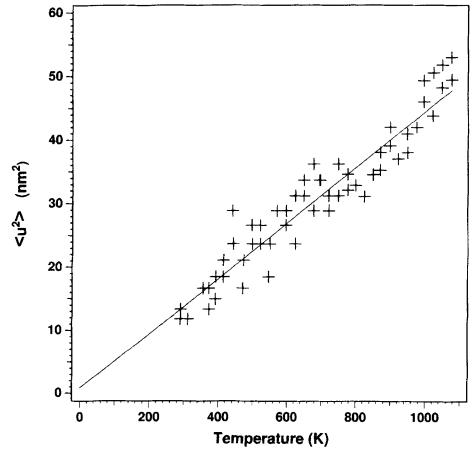

FIG. 2 Plot of the mean-square vibration amplitude versus temperature for a 5.1-μm-long, 16.6-nm-wide, free-standing nanotube. The slope is $0.044 \pm 0.0018\,\text{nm}^2\,\text{K}^{-1}$, giving an effective Young's modulus of 3.7 ± 0.2 TPa. The nanotube was heated from room temperature to 800 °C in steps of 25 °C. At each temperature, several low-magnification bright-field images of the vibrating tip were acquired on the slow-scan CCD camera at a resolution of 1.65 nm pixel. To improve contrast, a small objective aperture of semi-radius $0.7\,\text{nm}^{-1}$ was employed. The small aperture also increases the depth of focus, thereby minimizing the additional tip image blurring due to the vertical vibration of the nanotube. Images were collected with ~1,000 counts per pixel. Line traces were averaged over a 40 nm length at the nanotube tip. The room-temperature image profile of the base of the nanotube was convoluted with a gaussian to match the line trace of the tip.

sum of the variances

$$\sigma^2 = \frac{16L^3kT}{\pi Y(a^4 - b^4)} \sum_n \beta_n^{-4} \approx 0.4243 \frac{L^3kT}{Y(a^4 - b^4)} \qquad (4)$$

If we assume $a = 8\,\text{nm}$, $b = 1\,\text{nm}$, $L = 5{,}000\,\text{nm}$ and $Y = 5 \times 10^{11}\,\text{Pa}$ (which is typical for macroscopic carbon fibres[8]), then equation (4) gives a root-mean-square vibration amplitude of ~10 nm at room temperature, which agrees qualitatively with the observed blurring at the tip. An equivalent vibrational motion is occurring in the vertical direction, but we could not detect this motion in the TEM. In principle, there are also thermal longitudinal oscillations, and torsional modes. The mean square longitudinal thermal vibration amplitude is found from $\langle z^2 \rangle = LkT/\pi Y(a^2 - b^2)$, giving $\langle z^2 \rangle^{1/2} \approx 0.007\,\text{nm}$, which is negligible. The fundamental torsional mode generates a mean square twist $\langle \theta^2 \rangle = LKT/2\mu\pi(a^4 - b^4)$. Assuming that the shear modulus $\mu = Y/2(1 + \sigma)$, and that Poisson's ratio $\sigma \approx 0.3$, we find that $\langle \theta^2 \rangle^{1/2}$ is ~2 mrad. From equations (1)–(3), and the law of equipartition of energy, we expect each mode of the 'noisy' tip motion to follow $\langle u_n^2 \rangle^{1/2} \propto 1/f_n$ for an individual nanotube, with the constant of proportionality governed by $[L(a^2 - b^2)\rho]^{-1/2}$.

Because of the low image contrast at the tip, and the absence of the normal Fresnel fringes, great care is necessary to ensure that the nanotube tips are at the correct focus. Because the longitudinal vibration amplitudes at the end of the nanotube are small, spatial frequencies parallel to the fibre axis are not blurred. Consequently, Fresnel fringes at the top of the nanotube can be used to focus the vibrating tip. By measuring the change in focus between the base of the nanotube and the tip, it is possible to deduce the inclination of the nanotube to the horizontal. This assumption is reasonable because the droop of the nanotube under the influence of gravity, $u_g = L^4\rho g/2Y(a^2 + b^2)$, is less than 3×10^{-4} nm if we assume $\rho = 2{,}150\,\text{kg m}^{-3}$, and so the effect of gravity may be ignored.

The width of the tip image is essentially the convolution of the image of the relatively stationary nanotube base with the vibration profile. If we assume that the image profile of the (stationary) tip is similar to that at the base, then the vibration amplitude is obtained, in principle, by deconvoluting the base image profile from the tip image profile. In practice, as we know the form of the vibration profile, better results are obtained by convoluting the base profile with a gaussian and matching the result to the tip profile. For a given vibrating nanotube, the assumption of structural uniformity can be tested by comparing the total scattered intensity under the blurred tip image profile with that of the base. When the image focus is the same in each case, then the total scattering, as estimated by the area under the bright-field image profiles, should be identical. Discrepancies can be used to distinguish fibres with varying diameter along the length. For the nanotubes studied here, if the area under the scattering profile of the tip deviated by more than ±10% of that at the base, the data was rejected. In this study, we did not attempt to measure tip vibration frequencies. Spectral analysis of the undamped cantilever modes, which are expected to be among the lowest vibration frequencies of the nanotube, would provide an independent measure of Y through equation (3).

Figure 2 shows a graph of the measured mean-square vibration amplitude $\langle u^2 \rangle$ versus temperature T for a single nanotube. A good straight-line fit is obtained which yields a Young's modulus of $(3.7 \pm 0.2) \times 10^{12}$ Pa, which is about a factor of five higher than that measured for carbon fibres[5]. The intercept on the temperature axis occurs at $T_p \approx -13 \pm 29\,\text{K}$. This value implies that the electron beam, and other non-equilibrium perturbations, contribute $\approx +13\,\text{K}$ of additional heating, and confirms that non-equilibrium perturbations are small. Table 1 summarizes the results for a variety of nanotubes of different inner and outer diameters. We obtain an average value for Young's modulus, $Y = 1.8\,\text{TPa}$. Note that, on average, the measured modulus is highest for the thinner nanotubes. There is a full order-of-magnitude range in the values for Y. The spread in values stems partially from inevitable experimental uncertainties, such as in the estimation of the length of the tubes from their true point of anchoring, but most importantly from variation in structural features away from perfectly nested cylinders. For instance, should the nanotube have any inner ('bamboo-like') compartments with only the outer few layers being continuous from one end to the other, the hinging action at the joint will cause the modulus to be underestimated when we use equation (4). However, all these errors will tend to underestimate the flexural rigidity, or stiffness. We expect the correct modulus to tend towards the higher values.

It should be noted that the nanotube dimensions are optimal for direct observation of thermal vibrations. Therefore, the mechanical properties of other types of nanoscopic fibres, which are inaccessible to traditional techniques, could be studied by this method.

The values for the Young's modulus we find are much higher than those for typical carbon fibres[5]. For instance, an average value of 6.8×10^{11} Pa was obtained for macroscopic vapour-grown carbon fibres[8]. Carbon whiskers made by Bacon[9] had, so far, the highest measured extensional moduli of ~800 GPa. The in-plane modulus of single crystal graphite is of the order of 1 TPa. Therefore, by wrapping the graphite sheets into seamless cylinders, nanotubes appear to develop more stiffness than the graphite in-plane modulus would imply. Theoretical estimates predict in one case[2] that single-walled nanotubes might have a Young's modulus of the order of 5 TPa. Others, however, predict a softening of the nanotube with decreasing radius and show a distinct dependence on the helical pitch, the upper value being limited by that of planar graphite[3]. These studies neglect interlayer interactions which might contribute to a stiffening of the nanotubes.

Carbon fibres are already widely used in reinforced composites where high-strength light-weight materials are needed. As pointed out by Calvert[4], there is need for small-diameter, large-aspect-ratio fibres to obtain even higher-strength composites. Further, small-fibre composites should be easier to process[4]. In this context, the exceptional mechanical properties of nanotubes, combined with their small dimensions and large aspect ratio, could lead to optimal carbon-fibre-reinforced materials. □

Received 18 March; accepted 14 May 1996.

1. Ebbesen, T. W. *A. Rev. Mater. Sci.* **24,** 235–264 (1994).
2. Overney, G., Zhong, W. & Tomanek, D. *Z. Phys.* D**27,** 93–96 (1993).
3. Robertson, D. H., Brenner, D. W. & Mintmire, J. W. *Phys. Rev.* B**45,** 12592–12595 (1992).
4. Calvert, P. *Nature* **357,** 365–366 (1992).
5. Dresselhaus, M. S., Dresselhaus, G., Sugihara, K., Spain, I. L. & Goldberg, H. A. in *Graphite Fibers and Filaments* Ch. 6 (eds Gonser, U., Mooradian, A., Muller, K. A., Panish, M. B. & Sakaki, H.) 120–152 (Springer, New York, 1988).
6. Ebbesen, T. W. & Ajayan, P. M. *Nature* **358,** 220–222 (1992).
7. Kreyszig, E. *Advanced Engineering Mathematics* 7th edn. 643–644 (Wiley, New York, 1993).
8. Jacobsen, R. L., Tritt, T. M., Guth, J. R., Ehrlich, A. C. & Gillespie, D. J. *Carbon* **33,** 1217–1221 (1995).
9. Bacon, R. *J. appl. Phys.* **31,** 283–290 (1960).

ACKNOWLEDGEMENTS. We wish to thank M. E. Bisher for valuable assistance.